Applied Physics Letters

RESEARCH ARTICLE | JULY 06 2023

Extraordinary permittivity characterization of 4H SiC at millimeter-wave frequencies

Lei Li ; Steve Reyes ; Mohammad Javad Asadi ; Patrick Fay ; James C. M. Hwang

Appl. Phys. Lett. 123, 012105 (2023)
https://doi.org/10.1063/5.0148623

AIP Publishing

Applied Physics Letters ARTICLE pubs.aip.org/aip/apl

Extraordinary permittivity characterization of 4H SiC at millimeter-wave frequencies

Cite as: Appl. Phys. Lett. **123**, 012105 (2023); doi: 10.1063/5.0148623
Submitted: 1 March 2023 · Accepted: 23 June 2023 ·
Published Online: 6 July 2023

Lei Li,[1,a)] Steve Reyes,[2] Mohammad Javad Asadi,[1] Patrick Fay,[3] and James C. M. Hwang[1,4]

AFFILIATIONS

[1]School of Electrical and Computer Engineering, Cornell University, Ithaca, New York 14853, USA
[2]Anritsu Co., Morgan Hill, California 95037, USA
[3]Department of Electrical Engineering, The University of Notre Dame, Notre Dame, Indiana 46556, USA
[4]Department of Materials Science and Engineering, Cornell University, Ithaca, New York 14853, USA

[a)]**Author to whom correspondence should be addressed:** ll886@cornell.edu

ABSTRACT

For millimeter-wave power applications, GaN high-electron mobility transistors (HEMTs) are often grown epitaxially on a high-purity semi-insulating c-axis 4H-SiC substrate. For these anisotropic hexagonal materials, the design and modeling of microstrip and coplanar interconnects require detailed knowledge of both the ordinary permittivity $\varepsilon_{\perp}$ and the extraordinary permittivity $\varepsilon_{||}$ perpendicular and parallel, respectively, to the c-axis. However, conventional dielectric characterization techniques make it difficult to measure $\varepsilon_{||}$ alone or to separate $\varepsilon_{||}$ from $\varepsilon_{\perp}$. As a result, there is little data for $\varepsilon_{||}$, especially at millimeter-wave frequencies. This work demonstrates techniques for characterizing $\varepsilon_{||}$ of 4H SiC using substrate-integrated waveguides (SIWs) or SIW resonators. The measured $\varepsilon_{||}$ on seven SIWs and eleven resonators from 110 to 170 GHz is within ±1% of 10.2. Because the SIWs and resonators can be fabricated on the same SiC substrate together with HEMTs and other devices, they can be conveniently measured on-wafer for precise material-device correlation. Such permittivity characterization techniques can be extended to other frequencies, materials, and orientations.

High-purity semi-insulating c-axis hexagonal 4H SiC[1] is commonly used as the substrate for millimeter-wave GaN high-electron-mobility transistors (HEMTs) interconnected by microstrip transmission lines (microstrips) or grounded coplanar waveguides (GCPWs). This requires precise knowledge of the electrical permittivities of SiC at millimeter-wave frequencies to accurately predict the propagation delay and attenuation of waves along the transmission lines. For example, the quasi-transverse-electromagnetic (quasi-TEM) wave traveling on a microstrip or GCPW is governed by both ordinary permittivity $\varepsilon_{\perp}$ and extraordinary permittivity $\varepsilon_{||}$ perpendicular and parallel, respectively, to the c axis (Fig. 1). Although "static" $\varepsilon_{\perp}$ and $\varepsilon_{||}$ around 9.7[2] have been known for 6H SiC and are commonly used for 4H SiC, they are extrapolated from optical refractive indexes to millimeter-wave frequencies with large uncertainty and little regard to possible dispersion at millimeter-wave frequencies. Additionally, it has been shown that at optical frequencies, the permittivities, especially $\varepsilon_{||}$, of 4H SiC are higher than those of 6H SiC.[3,4] Note that the optical dielectric constant of 4H SiC around 6.6 is much lower than its dielectric constant at millimeter-wave frequencies, because the latter includes lattice vibrations that are cut off around 10 THz.[4] On the other hand, it is difficult to use conventional dielectric-characterization techniques to measure $\varepsilon_{||}$ alone or to separate $\varepsilon_{||}$ from $\varepsilon_{\perp}$.[4] As a result, there is little data for $\varepsilon_{||}$ of 4H SiC, especially at millimeter-wave frequencies [Fig. 2(a)].[5–10] Further, there is little report on the measurement uncertainty as illustrated in Fig. 2(b). Despite these uncertainties, many GaN/SiC process design kits provide a single effective ε_{EFF}, in which actual value may change with device geometry.

Conventionally, permittivity is characterized on bulk samples with on-axis waves,[4–11] making the characterization sensitive to the sample thickness, surface finish, and air gap.[11] By contrast, the present techniques are based on thin wafers and in-plane waves confined by lateral dimensions precisely defined by standard semiconductor processes. Therefore, the sample thickness and surface finish are less critical, and air gap is not of concern. Note that most semiconductor materials are available in the wafer form.

Contrary to the quasi-TEM wave in a microstrip or GCPW, the transverse electric (TE) wave propagating in a substrate-integrated waveguide (SIW) fabricated on c-axis 4H SiC is only governed by $\varepsilon_{||}$ [Fig. 1(d)], greatly simplifying its characterization. The wave is mostly confined in SiC with little radiation loss. The wave is distributed across

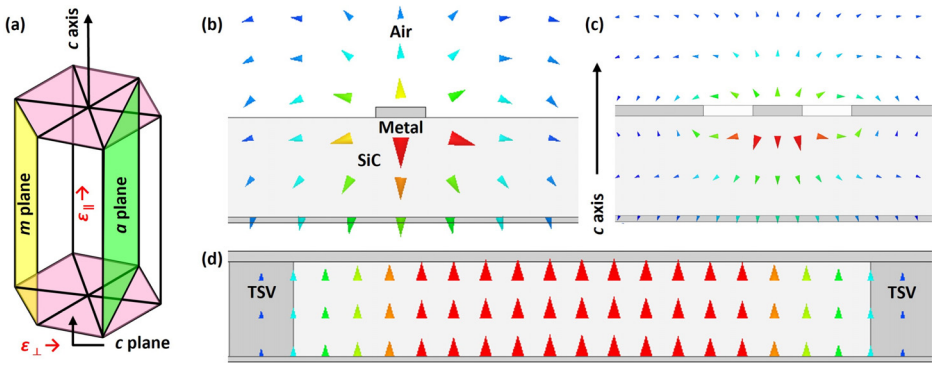

FIG. 1. (a) Crystal structure of 4H SiC. Simulated electric field distribution at 140 GHz in a (b) microstrip transmission line, (c) grounded coplanar waveguide, and (d) substrate-integrated waveguide on 100-μm-thick c-axis 4H SiC. Triangles point to the field direction. The warmer the color, the stronger the field.

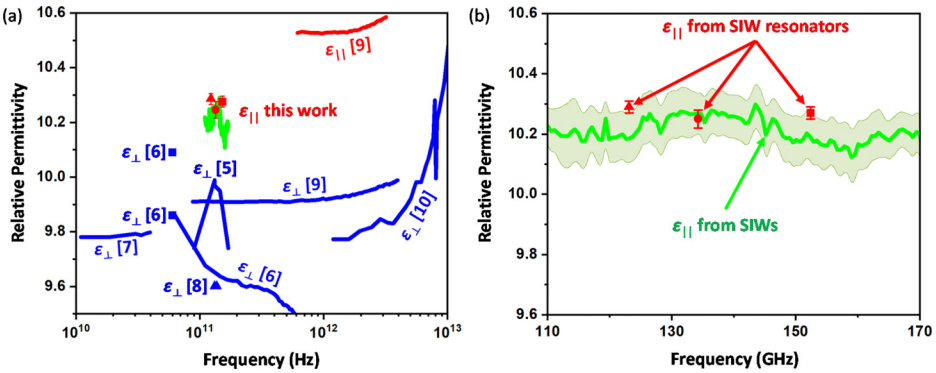

FIG. 2. (a) Relative ordinary permittivity $\varepsilon_\perp$ and extraordinary permittivity $\varepsilon_{||}$ from of 4H SiC. (b) Detailed view of data from this work. Vertical bars and shades indicate standard deviations.

the thickness of the SiC instead of concentrating on the surface as in a microstrip or GCPW, resulting in low dielectric loss. The SIW can be several times less lossy than a microstrip or GCPW fabricated on the same SiC substrate.[12] Taking advantage of these unique characteristics, this work explores SIWs and SIW resonators fabricated on the same SiC substrate as innovative techniques to characterize $\varepsilon_{||}$ and to fill a knowledge gap of the SiC permittivity.

Figure 3(a) illustrates the layout of two SIWs with the length $\ell = 860$ and 1100 μm, respectively, for fabrication (see the supplementary material) on 100-μm-thick high-purity semi-insulating c-axis 4H SiC. Each SIW is bound on the top and bottom with Ni-Al layers and on the left and right with two rows of through-substrate vias (TSVs). The TSVs have diameter of $d = 45$ μm and spacing of $s = 100$ μm center-to-center. Both SIWs have a width $w = 520$ μm (TSV center to TSV center) to cut off waves below 100 GHz. For wafer probing, the input and output of each SIW are transitioned to a GCPW. Each SIW-GCPW transition is 578-μm long, including a 175-μm GCPW section, a 353-μm tapered section, and a 50-μm SIW section.[13] In the GCPW section, the center electrode is 30-μm wide with a 16-μm gap from the ground electrodes. In the tapered section, the center electrode is linearly widened to 155 μm, while the gap is linearly widened to 158 μm, corresponding to a tapered gap with $\theta = 10°$ and $\varphi = 30°$ for the inner

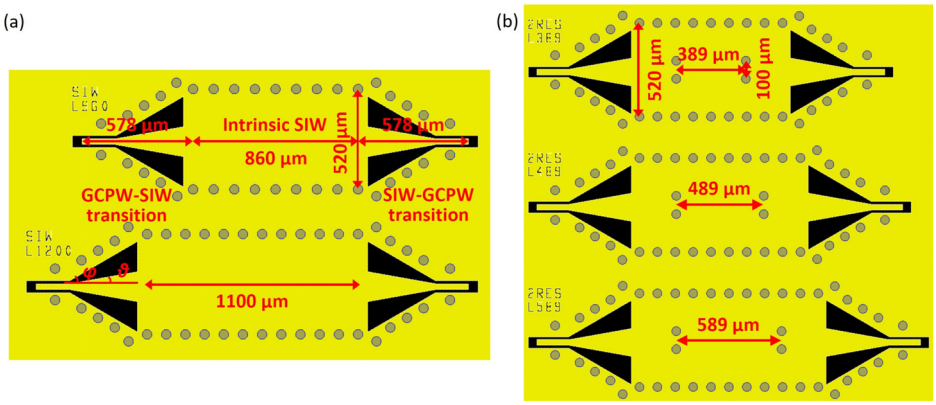

FIG. 3. Layouts of (a) SIWs and (b) SIW resonators of the same width but different lengths.

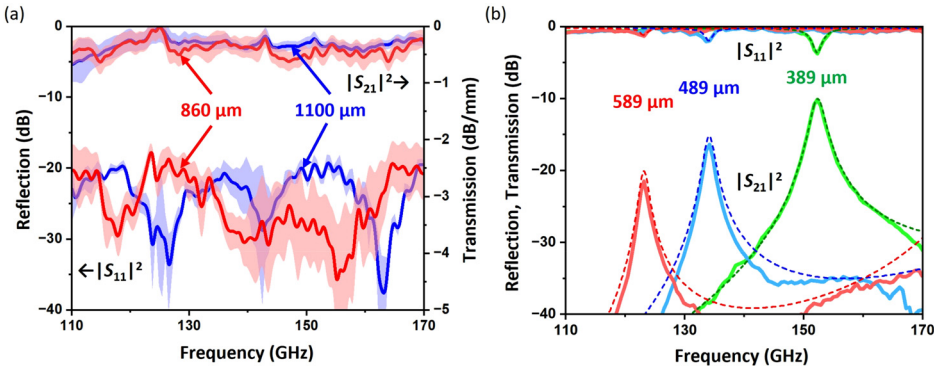

FIG. 4. (a) Measured intrinsic *S* parameters of (a) SIWs and (b) SIW resonators.

and outer angles, respectively. The transition has a low insertion loss (<0.2 dB) and a high return loss (>20 dB), which are critical to on-wafer characterization of the low-loss SIW.[14] Otherwise, the measurement uncertainty would be dominated by that of the transition.

Figure 3(b) illustrates the layout of three SIW resonators with $\ell = 389$, 489, and 589 μm, respectively, for fabrication together with the SIWs on the same SiC substrate. The length of each resonance cavity is determined by irises formed by a pair of TSVs spaced 100-μm apart in the middle of the SIW. All resonators are 520-μm wide and transitioned to GCPW at the input and output, the same as the SIWs.

Scattering (*S*) parameters are measured (see the supplementary material) across the D band (110–170 GHz) on four 860-μm-long SIWs, three 1100-μm-long SIWs, five 389-μm-long resonators, three 489-μm-long resonators, and three 589-μm-long resonators. The measured *S* parameters are de-embedded (see the supplementary material) past the GCPW-SIW transitions to the intrinsic SIW section. The de-embedding removes the effect of $\varepsilon_\perp$ embedded in the GCPW-SIW transitions, so that the de-embedded *S* parameters depend on $\varepsilon_{||}$ only.

Figure 4(a) shows the average magnitudes and standard deviations of the de-embedded reflection coefficient S_{11} and transmission coefficient S_{21} measured on the 860-μm and 1100-μm SIWs, with S_{21} normalized by the SIW length. It can be seen that the average insertion loss is less than 0.5 dB/mm across most of the D band, confirming the low loss of SIWs. The phase constant β of the propagating wave is simply the phase of the normalized S_{21}. Figure 5(a) shows that β averaged over the seven SIWs increases monotonically across the D band with weak nonlinearity, except the sharp cut off around 100 GHz. The standard deviation among the seven SIWs, being less than $\pm$ 0.06 rad/mm, is hardly visible.

The extraordinary permittivity $\varepsilon_{||}$ can be calculated from β at each frequency for each SIW by[15]

$$\varepsilon_{||} = \left[(\pi/w_{EFF})^2 + \beta^2\right](300/\omega)^2, \quad (1)$$

where ω is the angular frequency in GHz and $w_{\mathrm{EFF}} = 499$ μm is the effective SIW width according to[16]

$$w_{EFF} = w - (1.08/s - 0.1/w)d^2. \quad (2)$$

Figure 5(b) shows that $\varepsilon_{||}$ extracted from each of the four 860-μm-long SIWs and three 1100-μm-long SIWs are nearly constant with little dispersion, so that the average $\varepsilon_{||} = 10.21 \pm 0.10$. At each frequency across the D band, $\varepsilon_{||}$ is averaged over the seven SIWs and the standard deviation calculated as shown in Fig. 2(b). It can be seen in Fig. 5(a) that β calculated using a constant $\varepsilon_{||} = 10.2$ in Eq. (1) agrees with the measured β at each frequency.

The extracted $\varepsilon_{||}$ exhibits little dispersion probably because the D band is too high for dipolar relaxation yet too low for molecular/atomic resonances. 4H SiC has been reported to be highly transparent between 0.1 and 10 THz,[9] with weak absorption between 7 and 8 THz due to transverse acoustic phonons.[10] Below 7–8 THz, the lattice loss from two-phonon processes is small, unless there are lattice disorders, defects, impurities, or free carriers. Although a free-carrier absorption peak at 125 GHz has been reported for high-purity semi-insulating 4H SiC,[6] it is presently absent probably because of even higher purity.

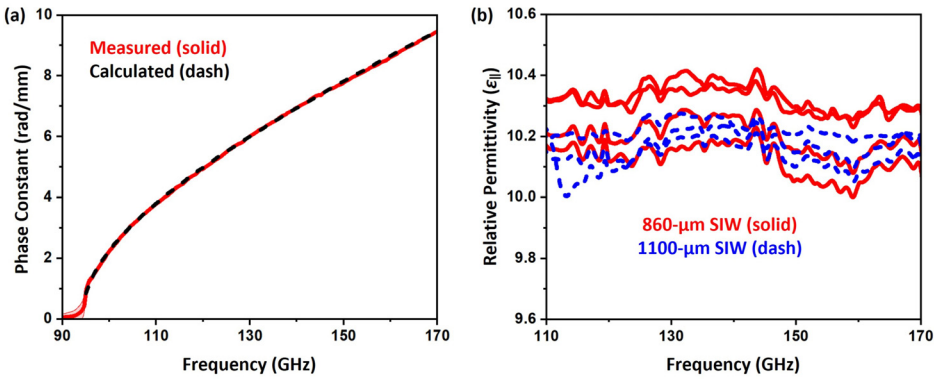

FIG. 5. (a) Measured phase constant β averaged over four 860-μm-long SIWs and three 1100-μm-long SIWs vs that calculated by using $\varepsilon_{||} = 10.2$. (b) Relative extraordinary permittivity measured on each of the seven SIWs.

Including the present $\varepsilon_{||}$ in Fig. 2(a), it can be seen to differ significantly from the reported millimeter-wave $\varepsilon_{\perp}$ or terahertz $\varepsilon_{||}$. The reason $\varepsilon_{||}$ is higher than $\varepsilon_{\perp}$ at the same frequency is probably because $\varepsilon_{\perp}$ is along the densest packed plane.

Figure 4(b) compares the measured and simulated magnitudes of S_{11} and S_{21} averaged for each resonator length. The simulation is performed by using the 3D finite-element full-wave simulator HFSS with automatic adaptive meshing and $\varepsilon_{||}$ as the only fitting parameter. It can be seen that $\varepsilon_{||} = 10.27$ and loss tangent $\tan\delta = 0.0001$[5,8] can fit resonators of all three lengths. Statistically, $\varepsilon_{||} = 10.29 \pm 0.02$ for the three 589-μm-long resonators, $\varepsilon_{||} = 10.25 \pm 0.03$ for the three 489-μm-long resonators, and $\varepsilon_{||} = 10.27 \pm 0.02$ for the five 389-μm-long resonators. These results are included in Fig. 2, which shows that they agree with $\varepsilon_{||}$ measured on the SIWs.

Recently, a special apparatus to induce in-plane waves in bulk materials has been developed for characterizing $\varepsilon_{||}$.[17] Although the apparatus appears to be still sensitive to sample thickness, surface finish, and air gap, it is nondestructive. Therefore, it will be interesting to characterize a sample with the apparatus and then fabricate the sample into SIWs for comparison with the present techniques. By contrast, the present techniques are conveniently based on wafer measurements without any special apparatus. However, it requires low-loss SIWs and SIW-GCPW transitions. Otherwise, the loss can not only add measurement uncertainties, but also trigger nonlinear phenomena to complicate the analysis. Presently, the SIW loss is dominated by the conductor loss instead of dielectric loss.[12] Therefore, the present techniques are unsuitable for characterizing small $\tan\delta$ as that of high-purity semi-insulating SiC.

In conclusion, enabled by the SIW, the above results confirm simple, accurate, and consistent on-wafer characterization of the extraordinary permittivity. Within measurement uncertainties, $\varepsilon_{||}$ was found to exhibit little dispersion. The measured $\varepsilon_{||}$ on seven SIWs and 11 SIW resonators is within $\pm 1\%$ of 10.2 across the D band. The resulted $\varepsilon_{||}$ fills a knowledge gap and differs significantly from the reported millimeter-wave $\varepsilon_{\perp}$ and terahertz $\varepsilon_{||}$. The present techniques can be extended to other frequencies, materials, and orientations. For example, SIWs can be fabricated on a-axis extract $\varepsilon_{\perp}$. The SIW width can be varied to characterize the permittivity at different frequency bands. Furthermore, because SIWs can be fabricated and measured together with other active and passive devices in close proximity on the same substrate, precise material-device correlation can be made. The material–device correlation can, in turn, help uncover other factors affecting device fabrication and reliability.

See the supplementary material for details of sample fabrication and measurement setup.[18,19]

This work was supported in part by the U.S. National Science Foundation (NSF) under Grant Nos. ECCS-2117305, ECCS-2122323, and ECCS-2132329, the U.S. Office of Naval Research under Grant No. N00014-21-1-2680, as well as the Semiconductor Research Corporation, and the U.S. Defense Advanced Research Projects Agency through the Joint University Microelectronics Program. This work was performed in part at the Cornell NanoScale Facility, an NNCI member supported by NSF Grant No. NNCI-2025233.

AUTHOR DECLARATIONS

Conflict of Interest

The authors have no conflicts to disclose.

Author Contributions

Lei Li: Investigation (lead); Writing – original draft (lead). **Steve Reyes:** Investigation (supporting). **Mohammad Javad Asadi:** Investigation (supporting). **Patrick J. Fay:** Investigation (supporting). **James C. M. Hwang:** Supervision (lead); Writing – review & editing (lead).

DATA AVAILABILITY

The data that support the findings of this study are available from the corresponding author upon reasonable request.

REFERENCES

[1]J. R. Jenny, S. G. Muller, A. Powell, V. F. Tsvetkov, H. M. Hobgood, R. C. Class, and C. H. Carter, Jr., J. Electron Mater. **31**, 366 (2002).
[2]J. L. Patrick and W. J. Choyke, Phys. Rev. B. **2**, 2255 (1970).
[3]P. T. B. Shaffer, Appl. Opt. **10**, 1034 (1971).
[4]O. P. A. Lindquist, K. Jarrendahl, S. Peters, J. T. Zettler, C. Cobet, N. Esser, D. E. Aspnes, A. Henry, and N. V. Edwards, Appl. Phys. Lett. **78**, 2715 (2001).
[5]J. M. Dutta, G. Yu, and C. R. Jones, in *Proceedings of Joint 31st International Conference on Infrared Millimeter Waves*, Shanghai, China (IEEE, 2006), p. 411.
[6]S. Chen, M. N. Afsar, and D. Sakdatorn, IEEE Trans. Instrum. Meas. **57**, 706 (2008).
[7]J. G. Hartnett, D. Mouneyrac, J. Krupka, J.-M. Le Floch, M. E. Tobar, and D. Cros, J. Appl. Phys. **109**, 064107 (2011).
[8]C. R. Jones, J. Dutta, G. Yu, and Y. Gao, J. Infrared. Milli. Terahz. Waves **32**, 838 (2011).
[9]M. Naftaly, J. F. Molloy, B. Magnusson, Y. M. Andreev, and G. V. Lanskii, Opt. Express **24**, 2590 (2016).
[10]A. T. Tarekegne, B. Zhou, K. Kaltenecker, K. Iwaszczuk, S. Clark, and P. U. Jepsen, Opt. Express **27**, 3618 (2019).
[11]See https://www.euramet.org/technical-committees/tc-projects/details/project/comparison-on-material-parameter-measurements-in-the-thz-spectral-range-with-optical-resonant-and-v/ for D. Allal, U. Arz, G. Gaumann, A. Gregory, M. Hudlicka, A. Kazemipour, T. Kleine-Ostmann, G. N. Phung, P. Marsik, M. Naftaly, H. Sakarya, X. Shang, D. Ulm, M. Wojciechowski, and P. Zagrajek, EURAMET TC Project Final Report (2022).
[12]L. Li, S. Reyes, M. J. Asadi, X. Wang, G. Fabi, E. Ozdemir, W. Wu, P. Fay, and J. C. M. Hwang, in ARFTG Microwave Measurement Conference, Las Vegas, NV, USA, 2023.
[13]M. J. Asadi, L. Li, W. Zhao, K. Nomoto, P. Fay, H. G. Xing, D. Jena, and J. C. M. Hwang, in *proceeding of IEEE MTT-S International Microwave Symposium (IMS)*, Atlanta, GA, USA (IEEE, 2021), p. 669.
[14]L. Li, S. Reyes, M. J. Asadi, D. Jena, H. G. Xing, P. Fay, and J. C. M. Hwang, in *ARFTG Microwave Measurement Conference*, Denver, CO, USA, 2022.
[15]S. Hu, Y. Xiong, J. Shi, L. Wang, B. Zhang, D. Zhao, T. G. Lim, and X. Yuan, in *Proceedings of IEEE Electronic Components and Technology Conference*, Las Vegas, NV, USA (IEEE, 2010), p. 46.
[16]F. Xu and K. Wu, IEEE Trans. Microwave Theory Techn. **53**, 66 (2005).
[17]Y. Kato and M. Horibe, IEEE Trans. Instrum. Meas. **68**, 1796 (2019).
[18]A. Davidson, K. Jones, and E. Strid, in *proceedings of ARFTG Conference Dig.*, Monterrey, CA (ARFTG, 1990), p. 57.
[19]R. B. Marks, IEEE Trans. Microwave Theory Techn. **39**, 1205 (1991).